Protein Science (1994), *3*:1020–1030. Cambridge University Press. Printed in the USA.

Phosphopeptide binding to the N-terminal SH2 domain of the p85α subunit of PI 3′-kinase: A heteronuclear NMR study

MEIKE HENSMANN,[1] GRANT W. BOOKER,[1,4] GEORGE PANAYOTOU,[2] JONATHAN BOYD,[1] JEFFREY LINACRE,[2] MIKE WATERFIELD,[2,3] AND IAIN D. CAMPBELL[1]

[1] Department of Biochemistry, University of Oxford, South Parks Road, Oxford OX1 3QU, United Kingdom
[2] Ludwig Institute for Cancer Research, London W1P 8BT, United Kingdom
[3] Department of Biochemistry and Molecular Biology, University College, London WC1E 6BT, United Kingdom

(RECEIVED February 2, 1994; ACCEPTED April 19, 1994)

Abstract

The N-terminal src-homology 2 domain of the p85α subunit of phosphatidylinositol 3′ kinase (SH2-N) binds specifically to phosphotyrosine-containing sequences. Notably, it recognizes phosphorylated Tyr 751 within the kinase insert of the cytoplasmic domain of the activated βPDGF receptor. A titration of a synthetic 12-residue phosphopeptide (ESVDY*VPMLDMK) into a solution of the SH2-N domain was monitored using heteronuclear 2D and 3D NMR spectroscopy. 2D-{^{15}N-^{1}H} heteronuclear single-quantum correlation (HSQC) experiments were performed at each point of the titration to follow changes in both ^{15}N and ^{1}H chemical shifts in NH groups. When mapped onto the solution structure of the SH2-N domain, these changes indicate a peptide-binding surface on the protein. Line shape analysis of 1D profiles of individual {^{15}N-^{1}H}-HSQC peaks at each point of the titration suggests a kinetic exchange model involving at least 2 steps. To characterize changes in the internal dynamics of the domain, the magnitude of the {^{15}N-^{1}H} heteronuclear NOE for the backbone amide of each residue was determined for the SH2-N domain with and without bound peptide. These data indicate that, on a nanosecond timescale, there is no significant change in the mobility of either loops or regions of secondary structure. A mode of peptide binding that involves little conformational change except in the residues directly involved in the 2 binding pockets of the p85α SH2-N domain is suggested by this study.

Keywords: dynamics; heteronuclear NMR; kinetics; ligand binding; PI 3′ kinase; SH2 domains

Src-homology 2 domains play a critical role in localizing intracellular-signaling molecules to activated growth-factor receptors (reviewed by Pawson & Schlessinger, 1993). A common immediate event in the binding of growth factors to their appropriate receptors is autophosphorylation of certain tyrosine residues in the cytoplasmic domains of these receptors (Schlessinger & Ullrich, 1992). SH2 domains bind to such phosphotyrosine sites, thereby mediating the association of activated receptors and signaling molecules containing SH2 domains, such as phospholipase C-γ (PLC-γ), ras-GTPase-activating protein (GAP), and phosphatidylinositol (PI) 3′ kinase (Cantley et al., 1991; Koch et al., 1991). A systematic binding study using a library of synthetic phosphopeptides has suggested that the sequence context of the phosphotyrosine determines its relative affinity for an SH2 domain, thus providing the specificity and selectivity of a particular SH2 domain for activated receptor subsites (Songyang et al., 1993).

PI 3′ kinase consists of an 85-kDa (p85α) regulatory subunit and a 110-kDa catalytic subunit. The p85α protein contains 2 SH2 domains. Two phosphotyrosine sites in the kinase insert of the cytoplasmic domain of the activated human βPDGF receptor, Tyr 740 and Tyr 751, are known to associate with these SH2 domains, conceivably with each tyrosine site engaging 1 of the 2 domains (Kashishian et al., 1992). Corresponding synthetic phosphotyrosine-containing peptides are able to block specifically the association of PI 3′ kinase with the PDGF receptor (Escobedo et al., 1991; Fantl et al., 1992). Analysis of kinetic parameters, using a biosensor-based system, has shown that the

Reprint requests to: Iain D. Campbell, Department of Biochemistry, University of Oxford, South Parks Road, Oxford OX1 3QU, UK; e-mail: idc@bioch.ox.ac.uk.

[4] Present address: Department of Biochemistry, University of Adelaide, Adelaide, Australia.

Abbreviations: SH2, src-homology 2; PDGF, platelet-derived growth factor; HSQC, heteronuclear single-quantum correlation; NOESY-HMQC, nuclear Overhauser enhancement multiple quantum coherence; States-tppi, States time-proportional phase incrementation method; PI, phosphatidylinositol.

affinity of the p85α SH2 domains for these peptides is very high, with dissociation constants of K_d = 30–100 nM (Panayotou et al., 1993). The specificity of the p85α SH2 domains for these sites has been attributed to the methionine residue in the third position (+3) relative to the phosphotyrosine (Cantley et al., 1991; Songyang et al., 1993).

Structural information is required to understand further how a particular SH2 domain selects for a particular phosphotyrosine site. The structures of the SH2 domains from the protein-tyrosine kinases Src and Lck, complexed with high-affinity peptides, have been determined by X-ray crystallography (Eck et al., 1993; Waksman et al., 1993). Two well-defined binding pockets on the protein surface appear to accommodate the tyrosine phosphate and the +3 residue, respectively, anchoring the peptide by a network of hydrogen bonds to these residues as well as to the peptide main chain.

The solution structure of the N-terminal SH2 domain of the p85α domain of PI 3′ kinase has previously been determined by NMR (Booker et al., 1992). Here, NMR is used to study the binding of Y751P$_{12}$ to the SH2-N domain in solution. The ^{1}H and ^{15}N spectra of the protein in the complex are assigned. Chemical-shift changes of the backbone amide ^{1}H and ^{15}N resonances are used to identify an interaction surface between the protein and its peptide ligand. Line shape and ^{15}N relaxation data are analyzed to give some information about the molecular dynamics of complex formation.

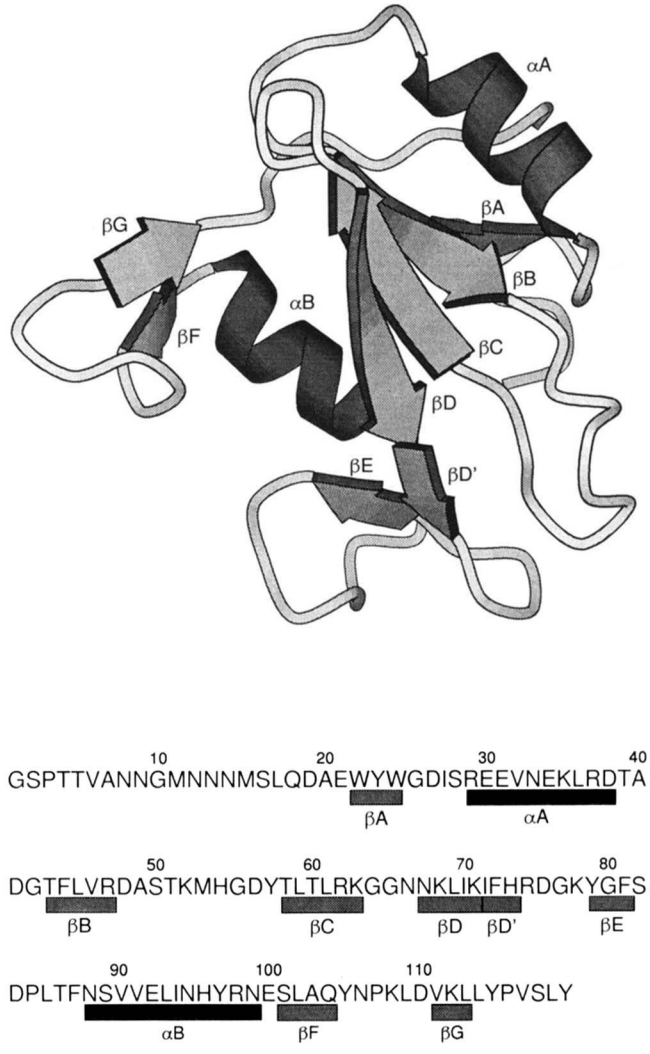

Fig. 1. MOLSCRIPT (Kraulis, 1991) diagram of the solution structure of the p85α SH2-N domain (Booker et al., 1993). The α-helices and β-strands are labeled according to the convention of Eck et al. (1993). The molecule is oriented so that the N- and C-termini lie at the back of the structure, behind helix αA and strand βA, respectively. The secondary-structural elements are also shown on the sequence of the protein, beneath the MOLSCRIPT figure.

Results

The solution structure and sequence of the N-terminal SH2 domain of p85α are represented in Figure 1 and Kinemage 1. Following the convention of Eck et al. (1993), the secondary-structural components are labeled βA, αA, βB-βE, αB, and βF-βG; loops will be referred to by the secondary-structural elements they join.

Mapping the chemical-shift changes

A 12-residue synthetic phosphopeptide, representing the SH2-binding site of activated PDGF receptor, was added to a 1.5 mM uniformly ^{15}N-labeled SH2 sample in 8 steps, achieving total peptide concentrations of 0.2, 0.4, 0.6, 0.8, 1.0, 1.3, 1.6, and 1.9 mM. A 2D-{^{15}N-^{1}H} HSQC experiment was performed at each peptide concentration. Saturation was achieved at a peptide concentration of 1.6 mM. Figure 2 shows a region of the spectra at peptide concentrations of 0 mM and 1.6 mM. Cross peaks represent the ^{15}N-^{1}H correlation for the backbone amide of each amino acid. It can be seen from the spectra that the chemical shifts of many resonances (such as Met 15 and Ile 27) are essentially unaltered by addition of the peptide, while large chemical-shift changes are observed for a number of residues (Glu 100 and Asp 56 shown). No resonances corresponding to residues 102, 104–106, 109, and 110, and no side-chain resonances corresponding to residues 81 and 82 could be assigned in the peptide-bound form; this is most likely due to extreme line broadening. To reassign significantly shifted peaks and to obtain complete ^{1}H resonance assignments, a 3D-NOESY-HMQC experiment was performed on the peptide-bound SH2-N domain (Tables 1, 2). The ^{1}H and ^{15}N resonance assignments of the SH2 domain with and without bound peptide could then be compared. Figure 3 shows the changes in ^{1}H shifts for NH and CaH groups and ^{15}N shifts for NH groups, as well as the magnitude of the vector over which the ^{15}N-^{1}H crosspeak is displaced (see Fig. 4). The residues for which assignments could not be made are represented by white bars. As can be seen in the figure, significant chemical-shift changes occur around residues Arg 29, Lys 71, and Phe 81, as well as in the BC loop. There are also some large changes for residues in the βF-FG-βG region, although for most of the FG loop these could not be mapped due to missing resonance assignments in the peptide-bound state (see above). Figure 5 and Kinemage 1 show the combined ^{15}N/NH displacements (Fig. 3D) translated into color on a backbone representation of the solution structure of the p85α SH2-N domain. The residues with the largest chemical-shift changes upon peptide binding clearly map to 1 side of the molecule. A backbone representation of the Y751P$_{12}$ peptide is

Table 1. *^{1}H and ^{15}N resonance assignments for the SH2 domain alone*[a]

Residue		NH	αCH	βCH	γCH	Other	^{15}N (NH)
1	G	x	x				x
2	S	x	x	x			x
3	P		x	x	x	x	x
4	T	8.07	x	x	x		119.90
5	T	8.21	x	x	x		119.38
6	V	8.08	x	x	x		x
7	A	8.32	x	x			122.13
8	N	8.36	x	x			120.25
9	N	8.45	x	x			120.54
10	G	8.37	x				118.31
11	M	8.11	x	x	x	x	120.49
12	N	8.39	x	x			120.48
13	N	7.97	x	x			121.46
14	N	8.37	x	x			x
15	M	8.03	4.46	x	x	x	120.70
16	S	8.47	x	x			120.14
17	L	8.36	3.55	1.30*	0.42	δδ′ 0.07, 0.34	121.90
18	Q	7.80	3.95	x	x		119.12
19	D	7.34	4.65	2.58, 2.85			119.82
20	A	7.51	3.94	0.14*			121.76
21	E	9.46	3.80	2.35*	2.26*		121.29
22	W	5.97	5.27	2.79, 3.88		2H 7.39; 4,5,6H 6.65; 7H 7.50; εNH 11.23	118.58
23	Y	7.29	5.63	2.64, 2.83		2,6H 7.52; 3,5H 6.62	121.29
24	W	8.80	4.15	2.58, 3.69		2H 7.49; 4H 7.68; 7H 7.08 5,6H 7.19; εNH 10.22	122.02
25	G	5.48	3.55, 3.77				122.66
26	D	8.58	4.90	2.85*			122.00
27	I	7.28	4.56	2.04	1.20, 1.51	δCH_3 0.56*; γCH_3 1.04*	120.25
28	S	8.55	4.57	4.16*			120.57
29	R	8.98	3.80	1.88, 1.95	1.64, 1.77	δδ′ 3.28*	120.71
30	E	8.85	4.09	2.05, 2.15	2.33, 2.55		120.43
31	E	7.87	4.05	1.95*	2.25*		120.89
32	V	8.01	3.10	2.27	0.87, 0.93		120.57
33	N	7.89	4.20	2.83, 2.97			119.92
34	E	7.61	4.10	2.15*	2.38*		120.44
35	K	7.70	4.01	1.52, 1.65	1.15, 1.30	δδ′ 0.89*; x	120.19
36	L	7.47	4.34	1.51, 1.77	1.77	δδ′ 0.58, 0.61	119.56
37	R	7.24	3.93	1.84, 1.96	1.61, 1.74	δδ′ 3.29*	121.46
38	D	8.09	4.43	2.84, 3.03			120.45
39	T	7.46	4.54	4.49	1.22*		118.18
40	A	8.26	4.41	1.47*			121.04
41	D	9.01	4.59	2.74, 2.94			121.13
42	G	9.27	3.96*				118.05
43	T	8.16	5.99	4.27	1.39*		121.08
44	F	8.56	6.03	2.88, 3.07		2,6H 6.85, 7.44; 3,5H 6.15, 6.69; 4H 6.46	121.03
45	L	8.66	5.00	2.20*	1.66	δδ′ 0.39, 0.62	119.22
46	V	9.71	5.35	2.55	1.14, 1.30		121.05
47	R	8.93	5.43	1.59, 1.71	2.40*	δδ′ 3.37*	121.34
48	D	8.93	5.00	2.57, 2.93			121.34
49	A	7.97	4.48	1.27*			121.52
50	S	x	x	x			x
51	T	7.62	4.43	2.93	1.25*		118.31
52	K	8.16	4.32	2.02*	1.30*	δδ′ 1.58*; εε′ 3.32*	120.71
53	M	8.02	4.46	2.15*	2.62*	x	120.27
54	H	8.46	4.77	3.29, 3.46		4H 7.34; x	120.31
55	G	8.26	3.94, 3.67				121.30
56	D	7.54	5.01	2.66*			120.28
57	Y	8.63	5.37	2.67, 3.31		2,6H 7.16; 3,5H 6.88	120.28
58	T	9.51	4.84	3.78	1.12*		119.94
59	L	9.48	5.00	2.24*	1.46	δδ′ 0.92*	118.06
60	T	9.12	5.49	3.78	1.02*		121.25
61	L	9.12	5.41	1.25, 1.59	1.50	δδ′ 0.68, 0.82	121.99
62	R	8.97	5.01	1.90, 2.43	1.66*	δδ′ 3.00	121.96

(*continued*)

Table 1. *Continued*

Residue	NH	αCH	βCH	γCH	Other	^{15}N (NH)
63 K	9.05	4.62	1.63, 1.75	1.50, 1.37	δδ′ 0.63, 0.82; x	120.04
64 G	10.47	4.01, 4.14				120.82
65 G	8.90	3.83, 4.15				122.67
66 N	7.51	4.95	2.67, 2.77			119.78
67 N	8.69	5.22	2.14, 2.79			120.50
68 K	9.60	4.61	1.77, 1.86	1.32, 1.50	δδ′ 0.80, 0.91; εε′ 2.76	121.68
69 L	8.52	5.00	1.72*	1.47	δδ′ 0.92	121.74
70 I	9.42	4.28	1.49	0.83, 1.05	γCH_3 0.29; δCH_3 0.45	121.85
71 K	8.51	4.41	1.72*	x	x; x	122.37
72 I	8.47	4.38	1.98	1.49, 1.66	γCH_3 0.91; δCH_3 1.13	121.09
73 F	8.94	4.90	2.92, 3.11		2,6H 7.35; 3,5H 7.54; 4H 7.42	122.03
74 H	8.58	5.63	2.88, 3.20		4H 6.41; x	120.17
75 R	8.29	4.13	1.71*	1.53, 1.58	δδ′ 3.21	121.83
76 D	9.19	4.31	2.64, 2.96			121.83
77 G	8.54	3.93, 4.22				122.44
78 K	7.57	5.37	1.39, 1.79	1.50, 1.57	x; εε2 ′ 3.03	120.34
79 Y	9.26	6.10	2.44, 2.79		2,6H 7.00; 3,5H 6.75	119.85
80 G	8.34	4.07, 4.66				122.41
81 F	9.27	5.44	2.51, 3.13		2.6H 6.87; 3,5H 6.51; 4H 6.42b	120.31
82 S	7.76	4.53	4.16, 4.20			118.46
83 D	8.27	4.61	2.47, 2.64			120.67
84 P		3.95	2.45*	2.07*	x	x
85 L	8.81	4.44	1.87*	1.00	δδ′ 0.63, 0.82	121.49
86 T	7.98	4.74	x	x		118.82
87 F	8.79	4.87	3.13, 3.21		2,6H 7.49; 4H 6.51; 3,5H 7.20b	120.82
88 N	9.74	5.18	3.13*			120.49
89 S	7.62	4.38	4.12, 4.26			118.38
90 V	8.22	3.19	1.60	0.26, 0.72		120.91
91 V	7.95	3.79	2.04	1.00, 1.13		120.37
92 E	7.94	4.15	2.25, 2.14	2.23*		120.29
93 L	7.06	2.71	1.80*	0.86	δδ′ 0.20, 0.41	120.88
94 I	8.12	3.35	1.71	1.24*	γCH_3 −0.22; δCH_3 0.24	120.44
95 N	8.66	4.37	2.86, 3.04			119.88
96 H	8.01	4.23	3.25*		x; x	120.52
97 Y	7.42	5.08	2.50, 3.60		2,6H 7.43; 3,5H 6.88	119.79
98 R	7.64	4.62	1.88*	2.09*	δδ′ 3.19	120.15
99 N	7.19	4.86	2.69, 2.87			119.26
100 E	7.63	4.51	1.45*	1.81, 2.25		120.76
101 S	8.43	4.39	3.89, 4.05			119.27
102 L	8.40	4.41	1.95, 2.27	1.57	δδ′ 0.34, 0.73	121.68
103 A	8.47	4.35	1.33*			121.29
104 Q	7.85	4.16	2.34*	2.63*		119.46
105 Y	7.97	4.77	3.12, 3.36		2,6H 7.09; 3,5H 6.78	120.57
106 N	7.94	4.39	2.16, 2.47			120.06
107 P		4.47	x	2.04*	δδ′ 3.73	x
108 K	7.92	4.33	2.00*	1.63, 1.75	δδ′ 1.57; x	x
109 L	8.28	4.33	x	x	x	x
110 D	7.94	4.05	2.86, 2.53			119.60
111 V	8.16	4.50	2.14	0.80*		121.23
112 K	7.67	4.78	1.68*	1.33, 1.51	δδ′ 1.02, 0.93	121.40
113 L	8.11	4.07	1.12, 1.35	0.34	δδ′ 0.29, −0.29	120.04
114 L	7.94	4.21	1.46*	0.95	δδ′ 0.32, 0.78	121.56
115 Y	7.79	5.61	3.20*		2,6H 7.21; 3,5H 6.97	119.95
116 P		3.50	1.80, 2.02	2.22, 2.45	δδ′ 3.87	x
117 V	7.97	4.17	2.10	0.85, 0.90		121.62
118 S	8.16	4.56	3.87, 3.99			121.10
119 L	8.50	3.93	0.78, 0.90	0.34	δδ′ 0.07, −0.07	121.91
120 Y	7.58	4.58	2.74, 3.26		2,6H 7.12, 3,5H 6.76	121.73

[a] Asterisks indicate degeneracy of methyl or methylene resonances; x denotes unassignable resonances.

Table 2. *^{1}H and ^{15}N resonance assignments for the SH2 domain complexed with $Y751P_{12}$*[a]

Residue	NH	αCH	βCH	γCH	Other	^{15}N (NH)
1 G	x	x				x
2 S	x	x	x			x
3 P		x	x	x	x	x
4 T	8.07	x	x	x		119.91
5 T	8.21	x	x	x		119.38
6 V	8.08	x	x	x		x
7 A	8.32	x	x			122.13
8 N	8.36	x	x			120.25
9 N	8.45	x	x			120.54
10 G	8.37	3.99, 4.70				118.31
11 M	8.11	x	x	x	x	120.49
12 N	8.39	x	x			120.45
13 N	7.97	x	x			121.43
14 N	8.35	x	x			x
15 M	8.00	x	x	x	x	120.70
16 S	8.43	x	x			120.10
17 L	8.32	3.52	1.25*	x	x	121.92
18 Q	7.78	3.91	2.02*	x		119.19
19 D	7.30	4.60	2.53, 2.80			119.77
20 A	7.46	3.90	0.08*			121.76
21 E	9.34	3.73	2.29*	2.18*		121.24
22 W	5.91	5.26	2.73, 3.83		2H 7.44; 4,5,6H 6.58; 7H x; εNH 11.15	118.56
23 Y	7.23	5.70	2.56, 2.73		2,6H 7.45; 3,5H 6.54	121.27
24 W	8.79	4.06	2.47, 3.60		2H 7.34; 4H 7.62; 7H 7.01 5,6H 7.19; εNH 10.13	122.00
25 G	5.36	3.46, 3.68				122.60
26 D	8.56	4.84	2.84*			122.00
27 I	7.23	4.56	1.92	1.41, 1.55	δCH_3 0.53*; γCH_3 0.98*	120.12
28 S	8.41	4.51	4.10*			120.34
29 R	8.94	3.72	1.77, 1.91	1.52, 1.77	δδ′ 3.17	120.54
30 E	8.67	4.04	2.06*	2.28, 2.47		120.37
31 E	7.84	3.99	1.92*	2.19*		120.88
32 V	8.00	3.02	2.20	0.84, 0.90		120.57
33 N	7.96	4.02	2.73, 2.91			120.00
34 E	7.51	4.01	2.09*	2.36*		120.42
35 K	7.52	4.00	1.42, 1.56	0.98, 1.20	δδ′ 0.76*; x	120.14
36 L	7.46	4.27	1.39, 1.70	1.70	δδ′ 0.49, 0.47	119.64
37 R	7.13	3.87	1.84, 1.90	1.62, x	δδ′ 3.25*	121.42
38 D	8.06	4.38	2.78, 3.00			120.42
39 T	7.40	4.46	4.40	1.14*		118.17
40 A	8.23	4.35	1.41*			121.05
41 D	8.95	4.54	2.67, 2.90			121.14
42 G	9.23	3.91*				118.08
43 T	8.08	5.88	4.21	1.31*		121.08
44 F	8.56	5.94	2.77, 3.06		2,6H 6.50, 7.30; 3,5H 6.08, 6.58; 4H 6.39	121.08
45 L	8.61	4.94	2.14*	1.54	δδ′ 0.24, 0.51	119.18
46 V	9.72	5.27	2.47	1.08, 1.25		121.05
47 R	9.06	5.43	1.36, 1.54	2.23*	δδ′ 3.46	121.31
48 D	8.89	4.99	2.53, 2.90			121.33
49 A	7.73	4.61	1.26*			121.45
50 S	10.66	4.22	x			120.64
51 T	7.06	4.29	x	1.24*		118.79
52 K	7.84	4.34	x	x	x; x	x
53 M	8.00	4.39	2.49	2.75	x	120.27
54 H	8.35	4.71	x, x		4H 7.34; x	120.31
55 G	8.30	3.61, 3.96				118.79
56 D	7.03	4.98	2.40, 2.61			120.12
57 Y	8.62	5.22	2.55, 3.23		2,6H 7.23; 3,5H 6.80	120.50
58 T	9.55	4.95	3.78	1.09*		120.22
59 L	9.61	4.97	2.62	1.40	δδ′ 0.90	118.18
60 T	9.05	5.44	3.68	0.87*		121.03
61 L	9.07	5.44	1.09, 1.52	1.50	δδ′ 0.46, 0.78	122.09
62 R	9.00	4.89	2.36, 2.85	1.57*	δδ′ 3.10	122.14

(*continued*)

Table 2. *Continued*

Residue	NH	αCH	βCH	γCH	Other	^{15}N (NH)
63 K	8.95	4.56	1.62, 1.72	1.54*	δδ′ 0.61, x; x	122.00
64 G	10.49	3.96, 4.10				120.78
65 G	8.83	3.74, 4.09				122.66
66 N	7.40	4.89	2.57, 2.74			119.71
67 N	8.62	5.05	2.02, 2.70			120.50
68 K	9.39	4.51	1.50, 1.87	0.93, 1.21	δδ′ 0.19, 0.51; εε′ 2.83	121.37
69 L	8.18	4.71	1.26*	0.87	δδ′ 0.44	121.48
70 I	9.12	4.62	1.52	0.85, 1.18	γCH_3 0.46; δCH_3 0.55	121.17
71 K	8.61	4.44	1.36*	x	x; x	122.42
72 I	8.28	4.34	1.57	0.93, 1.32	γCH_3 0.62; δCH_3 0.70	121.11
73 F	8.79	4.71	2.80, 2.96		2,6H 7.22; 3,5H 7.43; 4H 7.30	122.08
74 H	8.41	5.57	2.56, 3.21		4H 6.41; x	119.98
75 R	8.17	4.12	1.64*	1.47, 1.64	δδ′ 3.11	121.65
76 D	9.11	4.26	2.58, 2.93			121.66
77 G	8.40	3.88, 4.18				122.31
78 K	7.56	5.27	1.50, 1.70	1.32, 1.50	δδ′ x; εε′ 3.10	120.39
79 Y	9.25	6.05	2.35, 2.74		2,6H 7.04; 3,5H 6.63	119.93
80 G	8.24	3.99, 4.58				122.38
81 F	9.55	x	x, x		2.6H x; 3,5H x; 4H x	120.14
82 S	7.98	x	x, x			118.76
83 D	8.51	4.67	x, x			120.58
84 P		x	x	x	x	x
85 L	8.73	4.47	1.78	0.96	δδ′ 0.62, 0.75	121.32
86 T	8.17	4.52	x	x		118.82
87 F	8.72	4.82	3.08*		2,6H 7.48; 4H 6.50; 3,5H 7.19	120.82
88 N	9.71	5.10	3.08*			120.54
89 S	7.62	4.45	4.06, 4.28			118.36
90 V	8.16	3.13	1.50	0.20, 0.86		120.97
91 V	7.85	3.74	1.99	0.91, 1.11		120.35
92 E	7.85	4.05	2.24*	2.47*		120.27
93 L	7.07	2.80	1.75	0.82	δδ′ 0.21, −0.02	120.82
94 I	8.06	3.30	1.64	1.20*	γCH_3 −0.25; δCH_3 0.20	120.36
95 N	8.57	4.34	2.79, 2.97			119.77
96 H	8.00	4.34	3.13, 3.30		x; x	120.33
97 Y	7.34	4.78	2.42, 3.73		2,6H 7.50; 3,5H 6.83	119.56
98 R	7.35	4.62	1.89*	2.03*	δδ′ 3.16	120.16
99 N	7.15	4.91	2.54, 2.90			118.84
100 E	7.18	4.55	1.65*	1.85, 2.53		120.66
101 S	8.49	4.55	3.85, 4.01			119.71
102 L	x	x	x, x	x	δδ′ x, x	x
103 A	8.14	x	1.26*			120.77
104 Q	x	x	x	x		x
105 Y	x	x	x, x		2,6H x;3,5H x	x
106 N	x	x	x, x			x
107 P		x	x	x	x	x
108 K	8.24	4.34	1.95*	1.43, 1.56	δδ′ 1.56; x	119.73
109 L	x	x	x	x	x	x
110 D	x	4.03	x, x			x
111 V	8.22	4.48	2.03	0.70*		121.25
112 K	7.51	4.72	1.63*	1.26, 1.31	δδ′ 0.88*	121.38
113 L	7.95	4.04	1.04, 1.26	0.21	δδ′ 0.19*	x
114 L	7.79	4.02	1.36*	0.95	δδ′ 0.21, 0.95	121.54
115 Y	7.80	5.59	3.13*		2,6H 7.17; 3,5H 6.97	119.98
116 P		3.41	1.75, 2.00	2.23, 2.47	δδ′ 3.80	x
117 V	7.90	4.12	2.00	0.76, 0.80		121.60
118 S	8.44	4.45	3.81, 3.90			121.11
119 L	8.44	3.85	0.66, 0.85	0.19	δδ′ 0.00, −0.15	121.91
120 Y	7.56	4.50	2.68, 3.18		2,6H 7.04, 3,5H 6.18	121.69

[a] Asterisks indicate degeneracy of methyl or methylene resonances; x denotes unassignable resonances.

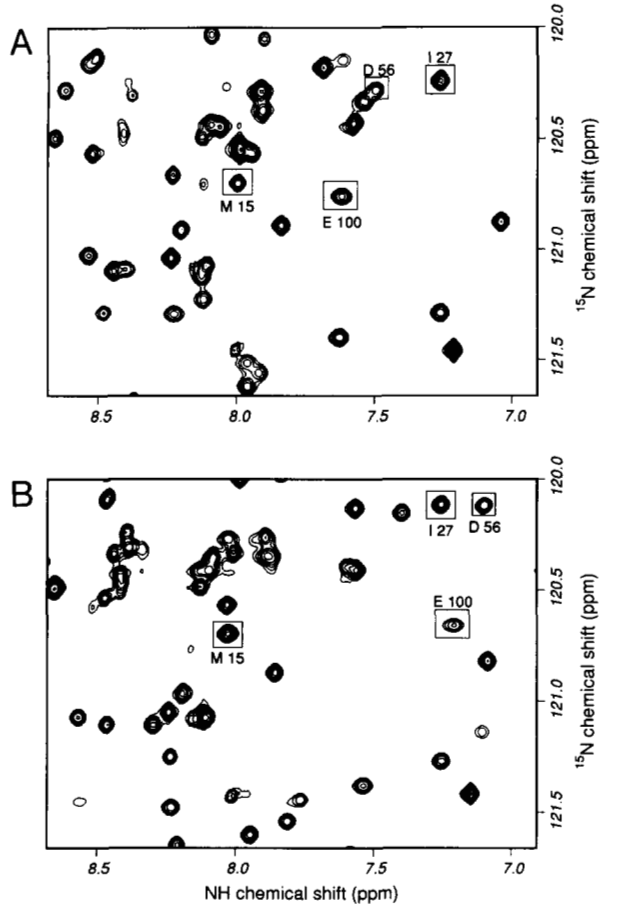

Fig. 2. Region of the 2D-{^{15}N-^{1}H} HSQC spectrum at peptide concentrations of **(A)** 0 mM and **(B)** 1.6 mM. Crosspeaks represent the correlation between the ^{15}N and NH resonances of each amide group. Several peaks are labeled to demonstrate how the chemical shifts of different residues are affected to various degrees. The peaks corresponding to the backbone amides Asp 56 and Glu 100 are displaced significantly, the one corresponding to Ile 27 slightly less, whereas that of Met 15 does not change position.

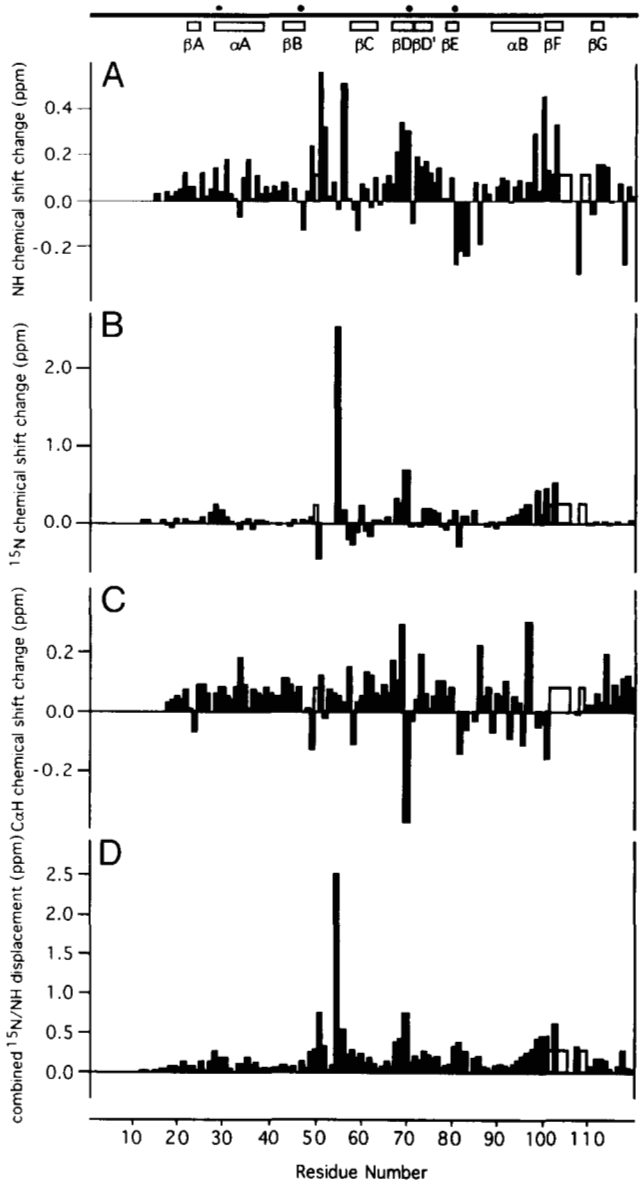

Fig. 3. Plots of the chemical-shift changes of main-chain **(A)** NH, **(B)** ^{15}N, and **(C)** CaH resonances, as well as **(D)** the combined ^{15}N/NH displacement (see Fig. 4) versus the amino acid sequence of the p85α SH2-N domain. At the top of the figure, the position of secondary-structural elements is indicated by boxes, whereas residues that have been implicated in anchoring the phosphotyrosine (Arg 29, Arg 47, Lys 71) and the (+3) methionine (Phe 81) of the peptide are marked by black circles. (See Figure 1 for details of sequence and location of secondary-structural elements.) Residues for which no resonances could be assigned in either the free or the peptide-bound state are indicated by white bars of arbitrary height in the plots.

modeled into the structure in the right-hand part of the figure, analogous to the position of the peptide in the Lck-SH2 structure (Eck et al., 1993).

Kinetic analysis

The changes in line shape and intensity of each resonance through the titration can be analyzed to give information about the kinetics of the complex formation. Figure 6 shows the overlay of the 1D profiles of the peaks corresponding to the amide proton or ^{15}N resonances of Glu 100 and Lys 68, respectively, at each peptide concentration. These profiles are representative for those residues in the protein that exhibit significant chemical-shift changes. As can be seen in the figure, the peak at the resonance corresponding to the residue in the free protein (P) exhibits decreasing intensity, strong broadening, and a change in chemical shift as the peptide concentration increases. The peak at the resonance corresponding to the residue in the protein with bound peptide (PL) shows increasing intensity, decreasing line width, and, in the case of Lys 68, a small change in chemical shift.

Computer simulations of a simple 2-site chemical exchange (Fig. 7A) and of a linear 3-site exchange (Fig. 7B) were carried out. The 2-site exchange model describing simple 1-step binding cannot account for the kind of chemical-shift changes of the P peak illustrated in Figure 6. Simulations using the 3-site exchange model (2-step binding with species PL and PL*) can pro-

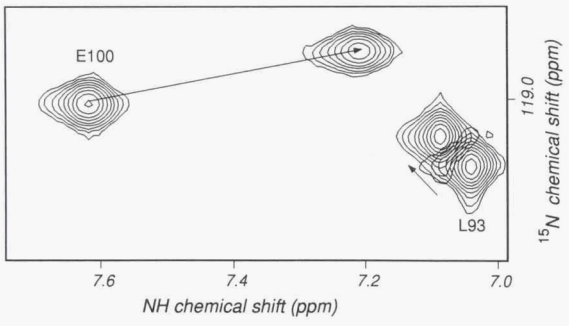

Fig. 4. Overlay of a region of the 2D-{^{15}N-^{1}H} HSQC spectra at peptide concentrations of 0 mM and 1.6 mM. Arrows indicate the magnitudes of the combined ^{15}N/NH displacement for the respective peaks. A plot of these displacements versus the residue number of each amide ^{15}N-^{1}H spin pair is shown in Figure 3D.

duce chemical-shift changes for the P peak, although shifts in the PL peak still cannot be reproduced. The kinetic mechanism of peptide binding must therefore involve at least 2 steps, possibly an encounter step followed by loop closure.

Dynamic behavior

To investigate internal mobility of the SH2-N domain the ^{15}N-^{1}H heteronuclear NOE was measured using uniformly ^{15}N-labeled protein in the absence and presence of synthetic phosphopeptide at 2 different field strengths, 500 and 600 MHz. Because the magnitude of this NOE is dependent on correlation time, it can be used as a measure of backbone mobility (Kay et al., 1989) (the ^{15}N NOE values expected for isotropic motion of a protein with correlation time 7 ns are 0.79 at 500 MHz and 0.81 at 600 MHz). Loops between secondary-structure elements often have a high intrinsic mobility and their backbone amides show correspondingly low ^{15}N NOE values (e.g., Main et al., 1992). Figure 8 shows the NOE profile against the sequence both for the apo and holo proteins at 2 different ^{1}H frequencies. Apart from negative NOEs at the N-terminus, which indicate disordered motion there, none of the loops exhibit consistently lower NOEs at either frequency than that expected for isotropic motion. There is some suggestion, from the 500-MHz data, that the loops 50–55 and 80–83 are somewhat mobile in the absence of peptide, but this effect is extremely small.

Discussion

Chemical-shift perturbations upon ligand binding have proven to be a reliable and sensitive probe for the ligand binding site of a protein (reviewed by Otting, 1993). Because the chemical-shift changes measured here concern the backbone amide groups, they are likely to reflect any changes in conformation and/or hydrogen bonding due to peptide binding. The results are consistent with the Y751P$_{12}$ peptide binding across 1 face of the p85α SH2-N domain, in a very similar manner to the complex observed for both the Src- and Lck-SH2 domains (Eck et al., 1993; Waksman et al., 1993). The large chemical-shift changes at and around residues Arg 29, Lys 71, and Phe 81 imply that these may indeed be anchoring residues in the binding pockets for the phosphotyrosine and the (+3)-methionine, respectively, as suggested by Waksman et al. (1993).

The BC loop is also clearly involved in peptide binding. The Ser 50 ^{15}N-^{1}H crosspeak, which could not be assigned in the {^{15}N-^{1}H}-HSQC spectrum of the SH2-N domain without peptide, is observed far downfield in the spectrum upon peptide binding, and the Gly 55 crosspeak experiences the largest chemical-shift change in the ^{15}N dimension. These residues lie at each end of the BC loop. In contrast, the ^{15}N and ^{1}H resonances for residues Met 53 and His 54 show virtually no chemical-shift change. These results are consistent with a hinge-like movement of this loop upon peptide binding, similar to that observed in the crystal structures of free and complexed Src-SH2 (Eck et al., 1993; Waksman et al., 1993). This is also consistent with the increased protection of the BC loop from proteolysis, in the presence of peptide, observed by Shoelson et al. (1993).

The kinetics of the interaction between SH2 domains and phosphotyrosine-containing sequences have been investigated in an earlier study employing a surface plasmon-resonance approach using a BIAcore system (Felder et al., 1993; Panayotou et al., 1993). In those experiments, phosphotyrosine-containing peptides were immobilized on a biosensor surface. The association rates of recombinant SH2-domain fusion proteins to this surface were measured. Bound protein was then released by

Fig. 5. Combined ^{15}N/NH chemical-shift changes (Fig. 3D) mapped onto a backbone representation of the solution structure of the p85α SH2-N domain (Booker et al., 1993). Colors indicate the following ranges: blue, <0.1 ppm; yellow, 0.1–0.25 ppm; orange, 0.25–0.5 ppm; red, >0.5 ppm. Magenta marks residues for which no ^{15}N or NH resonance assignments could be obtained in the free (Ser 50) or peptide-bound form (Leu 102, Gln 104, Tyr 105, Asn 106, Leu 109, and Asp 110) of the protein, as well as those with severely broadened ^{15}N-^{1}H HSQC crosspeaks (Phe 81 and Ser 82). Prolines are colored gray. On the right-hand side of the figure a backbone model of the Y751P$_{12}$ peptide is modeled onto the structure based on the position of the peptide in the Lck complex (Eck et al., 1993).

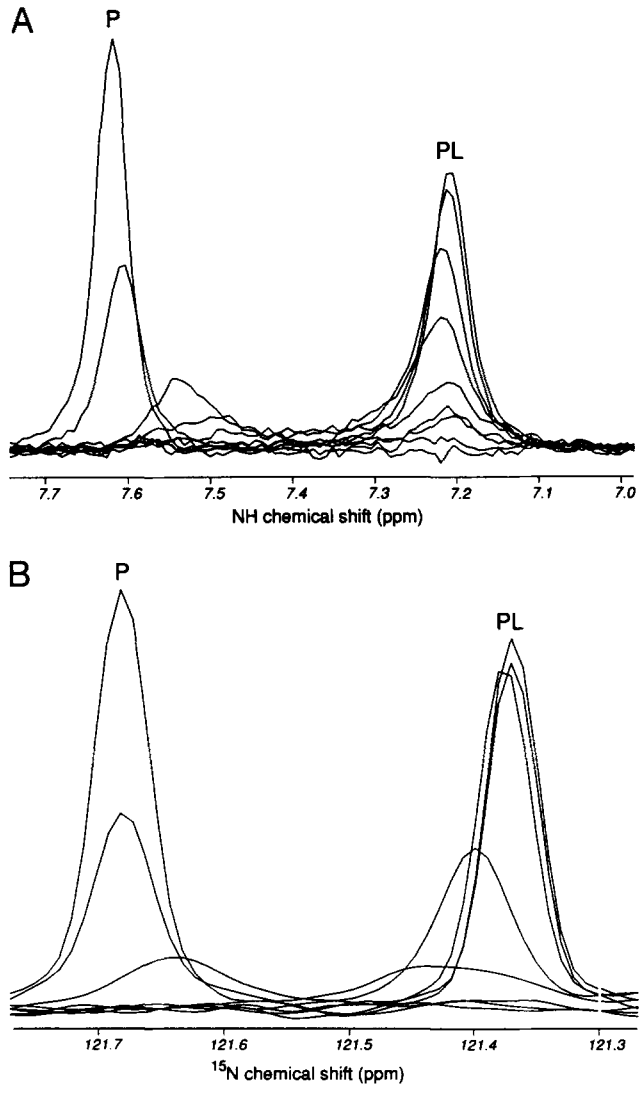

Fig. 6. Superposition of the 1D profiles for residues (**A**) Glu 100 (NH dimension) and (**B**) Lys 68 (^{15}N dimension) at each peptide concentration. For both residues, no significant chemical shift change is observed in the respective other dimension. The chemical shifts of the resonances in the free and peptide-bound state of the protein are labeled P and PL, respectively. The changes in intensity and chemical shift of the resonances at each position are representative for those of the majority of the significantly shifted residues in the protein.

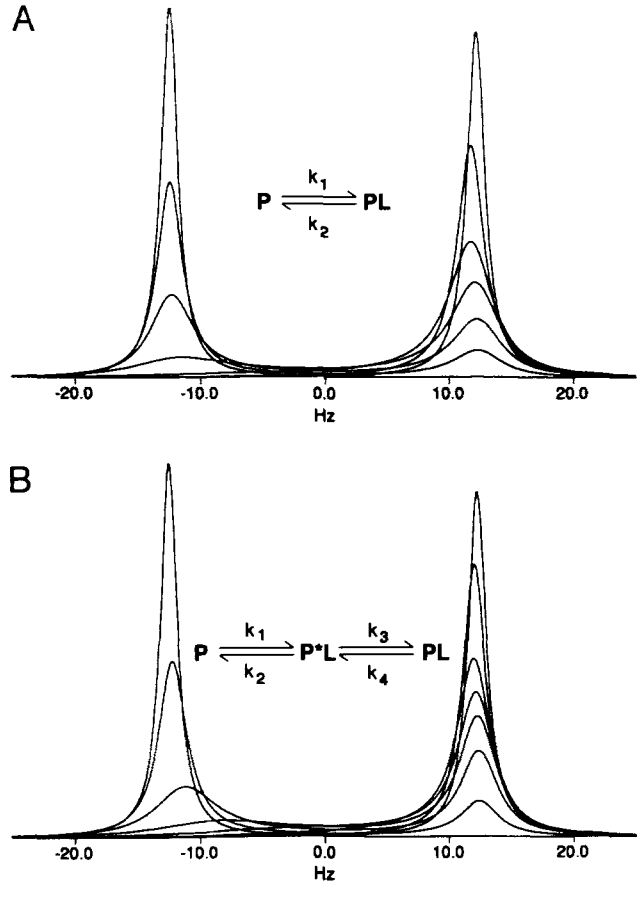

Fig. 7. Simulations of (**A**) a simple 2-site chemical exchange and (**B**) a linear 3-site exchange. In both the separation between sites P and PL is set to 25 Hz, and the line width of each peak to 2.5 Hz, which closely corresponds to the parameters observed in Figure 6A. For the 2-site exchange, k_2 is set to 10 s^{-1} and k_1 is varied. For the 3-site exchange, $k_3 = 50\ s^{-1}$, $k_4 = 10\ s^{-1}$, $k_2 = 100\ s^{-1}$, and k_1 is varied and the frequency of site P*L is set to be 2 Hz larger than that of site PL.

washing with increasing amounts of free competitive peptide to measure dissociation rates. The results for the p85α SH2-N domain and a synthetic 17-mer phosphopeptide corresponding to the Y751 site suggest an association rate constant of 3.34×10^6 $M^{-1}\ s^{-1}$ and a dissociation rate constant of 0.14 s^{-1} (dissociation constant $K_d = 42$ nM in the presence of 20 μM competing peptide). These rates are significantly slower than the ones suggested by line shape analyses of the kind shown in Figure 7. The difference could arise from temperature and pH changes but could also be due to technical differences. The BIAcore technique makes separate measurements of "on" and "off" rates at a surface, whereas the NMR method is a direct measurement of exchange at equilibrium. Our study has also indicated that the binding mechanism involves at least 2 steps.

The ^{15}N NOE data, which detect motion on a nanosecond time scale, do not indicate very significant changes in mobility in loop regions on peptide binding. There is, however, considerable line broadening observed around residues 55, 81, and 105 in the presence of peptide. This may be consistent with the multistep binding implied by the line shape analysis in Figure 7, with loop movements on a millisecond time scale causing the broadening. Interestingly, these slower loop movements seem to affect the specificity determining the methionine (+3) pocket considerably more than the phosphotyrosine pocket.

Thus, although the ^{15}N NOE experiment detected little change, on a nanosecond time scale, between peptide-bound and peptide-free states, the additional line broadening observed in the presence of peptide suggests some loop movement and changes on a slower time scale. There is, however, no evidence for a significant global conformational change in the protein upon peptide binding. For the majority of residues, the ^{1}H and ^{15}N chemical-shift values do not change significantly. Furthermore, even for shifted resonances, the pattern and intensities of intramolecular NOEs in 3D-NOESY-HMQC spectra remain essentially unaltered upon peptide binding (results not shown).

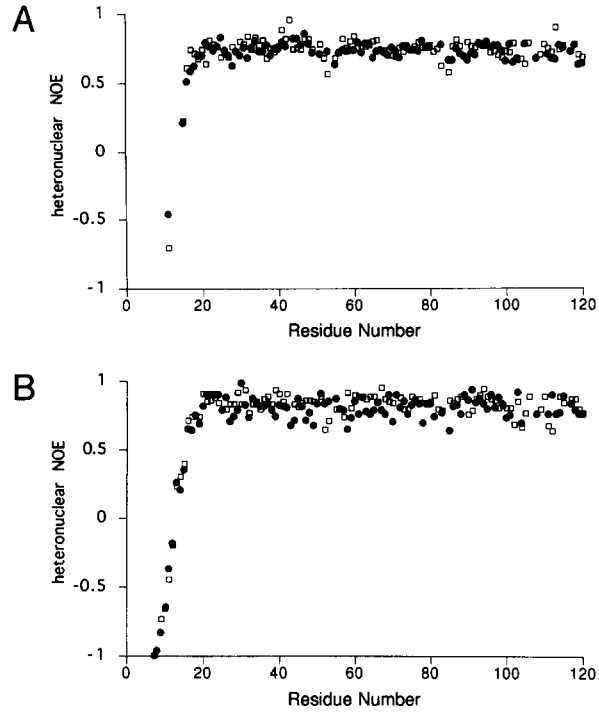

Fig. 8. Plots of the heteronuclear {^{15}N-^{1}H} NOE versus the residue number of each amide ^{15}N-^{1}H spin pair of the p85α SH2-N domain without the peptide (squares) and saturated with Y751P$_{12}$ peptide (circles). NOEs were measured at 2 different ^{1}H frequencies: **(A)** 500 MHz and **(B)** 600 MHz. No values were obtained for His 54 because its ^{15}N and ^{1}H resonances overlap with those of an N-terminal residue (Asn 14). In both A and B, no values are plotted for unassigned residues.

This suggests that secondary-structural elements and tertiary organization are preserved.

Two earlier studies reported some conformational change between free and complexed SH2 domains. Panayotou et al. (1992) observed significant fluorescence and CD spectral differences upon formation of a complex with a 17-residue Tyr 751 phosphopeptide. These could, however, not be related to any particular part of the protein structure. Shoelson et al. (1993) observed chemical-shift changes of the Trp 22 and Trp 24 sidechain resonances in 1D-NMR spectra. When proper assignment of these residues and the size of the observed chemical-shift change (smaller than 0.1 ppm) are considered, it seems unlikely that these residues undergo a significant conformational change.

Synthetic phosphopeptides corresponding to the Y-X-X-M motif on the PDGF receptor, IRS-1, and mT antigen have been shown to stimulate PI 3-kinase activity (Backer et al., 1992; Carpenter et al., 1993). This suggests that phosphopeptide binding to SH2 may effect a structural change in the p85 regulatory subunit of PI 3-kinase that is somehow transmitted to the p110 catalytic subunit. The experiments are, however, not conclusive as to whether engagement of 1 of the 2 SH2 domains of p85 is sufficient for the observed activation. It is conceivable that simultaneous phosphopeptide binding of both domains is necessary to bring about activation. Because the results presented here do not indicate a large peptide-induced conformational change in an isolated SH2-N domain, studies of intact protein or larger protein fragments will be necessary to elucidate fully the role of conformational changes in the activation of PI 3-kinase.

In conclusion, the results presented here suggest that phosphopeptide binds to SH2-N domains in at least 2 steps, with loops closing around the peptide after the initial encounter step. There is little evidence, however, that the global conformation of the SH2 domain changes significantly on peptide binding. The results are consistent with peptide recognition in the manner of the 2-plug socket model suggested by the crystal structures of Src and Lck SH2–peptide complexes.

Materials and methods

Protein and peptide preparation

^{15}N-enriched SH2 samples were prepared as previously described (Booker et al., 1992) using bacterial expression of GST-fusion protein in appropriately transformed *Escherichia coli* BL21 cells grown in minimal medium (Maniatis et al., 1982). Phosphorylated peptides were prepared as previously described (Panayotou et al., 1992), using 9-fluorenylmethoxycarbonyl (Fmoc) chemistry on an Applied Biosystems 430A peptide synthesizer. Subsequent tyrosine phosphorylation of the peptide EVDYVPMLDMK was performed by incubation with epidermal growth factor-stimulated plasma membranes as described (Panayotou et al., 1992).

NMR experiments

The sample for NMR spectroscopy was prepared by dissolving the uniformly ^{15}N-labeled protein in 0.5 mL of 50 mM sodium phosphate (pH 5.8) containing 5% (v/v) D_2O to a concentration of 1.5 mM. Samples of peptide for the titration studies were prepared by lyophilizing aliquots of an aqueous peptide solution of known concentration (determined by amino acid analysis). The lyophilized aliquots were then added to the 0.5-mL SH2 sample in 8 steps, each step increasing the peptide concentration of the sample by 0.2 or 0.3 mM.

Experiments were performed on 2 homemade spectrometers operating at ^{1}H frequencies of 500 MHz and 600 MHz, respectively. All spectra were recorded at 35 °C. In all experiments, trim pulses were used for solvent signal suppression and ^{15}N decoupling during acquisition was achieved by GARP-1 phase modulation (Shaka et al., 1985). Sign discrimination in t_1 was achieved using the States time-proportional phase incrementation method (Marion et al., 1989).

Two-dimensional {^{1}H-^{15}N} ^{1}H-detected single-quantum heteronuclear chemical-shift correlation spectra (Bodenhausen & Ruben, 1980; Norwood et al., 1990) were acquired at 500 MHz with 1,024 t_2 data points, 256 t_1 increments, and spectral widths of 7,017 Hz (^{1}H) and 2,500 Hz (^{15}N), respectively. The 2-dimensional heteronuclear {^{1}H-^{15}N} NOE spectra (Kay et al., 1989) were acquired with spectral widths of 30,303 Hz and 2,500 Hz (500 MHz) or 36,363 Hz and 2,444 Hz (600 MHz) in the ^{1}H and ^{15}N dimensions, respectively. A total of 4,096 t_2 data points and 256 t_1 increments were collected at both frequencies.

Three-dimensional ^{1}H NOE ^{15}N-^{1}H heteronuclear multiple quantum coherence experiments (Messerle et al., 1989; Driscoll et al., 1990) were performed with States-tppi acquisition in both the t_1 and t_2 dimensions. A total of 64 t_3 (^{15}N) planes with 512 t_2 (^{1}H) data points and 128 t_1 (^{1}H) increments at a spectral width of 7,017 Hz were recorded with a mixing time of 150 ms.

All data were processed on Sun workstations using the Felix 2.1 software package (Hare Research, Inc.). Skewed and phase-shifted sine-bell weighting functions as well as zero-filling were applied before Fourier transformation. For the 3D-NOESY-HMQC spectra, linear prediction was applied in the ^{15}N dimension.

Line shape analysis

The simulations of the NMR line shapes involved numerical solution of a set of coupled differential equations of the form

$$d\mathbf{X}/dt = \mathbf{AX} = [i\boldsymbol{\omega} + \mathbf{R} + \mathbf{K}]\mathbf{X},$$

where **X** is a column vector and the matrix **A** is composed of the sum of the diagonal matrices $\boldsymbol{\omega}$ and **R**, containing the chemical-shift and relaxation data, respectively. **K** is an exchange matrix, containing information about forward and backward rate constants (Sack, 1958; Abragam, 1961).

The complex solutions to these equations were obtained using NAG library routines (NAG Group Ltd., Oxford, UK). The simulations used either a 2- or 3-site exchange model as indicated in Figure 7. Chemical shifts, transverse relaxation rates, and individual rate constants were input for each species. The solutions were used to simulate free induction decays, which were processed in the same way as the experimental data to allow direct comparison.

Acknowledgments

We thank Dr. C.J. Morton for technical assistance and helpful discussions and Oanh Truong for peptide synthesis. This work is a contribution from the Oxford Centre for Molecular Sciences that is supported by the MRC and SERC. G.W.B. was supported by Zeneca through a LINK Protein Engineering Programme. The support of the Wellcome Trust is also gratefully acknowledged.

References

Abragam A. 1961. *Principles of magnetic resonance*. Oxford, UK: Oxford University Press.

Backer JM, Myers MG Jr, Shoelson SE, Chin DJ, Sun XJ, Miralpeix M, Hu P, Margolis B, Skolnik EY, Schlessinger J, White MF. 1992. Phosphatidylinositol 3′-kinase is activated by association with IRS-1 during insulin stimulation. *EMBO J 11*:3469–3479.

Bodenhausen G, Ruben DJ. 1980. Natural abundance nitrogen-15 NMR by enhanced heteronuclear spectroscopy. *Chem Phys Lett 69*:185–189.

Booker GW, Breeze AL, Downing AK, Panayotou G, Gout I, Waterfield MD, Campbell ID. 1992. Structure of an SH2 domain of the p85α subunit of phosphatidylinositol-3-OH kinase. *Nature 358*:684–687.

Cantley LC, Auger KR, Carpenter C, Duckworth B, Graziani A, Kapeller R, Soltoff S. 1991. Oncogenes and signal transduction. *Cell 64*:281–302.

Carpenter CL, Auger KR, Chanudhuri M, Yoakim M, Schaffhausen B, Shoelson S, Cantley LC. 1993. Phosphoinositide 3-kinase is activated by phosphopeptides that bind to the SH2 domains of the 85-kDa subunit. *J Biol Chem 268*:9478–9483.

Driscoll PC, Clore GM, Marion D, Wingfield PT, Gronenborn AM. 1990. Complete resonance assignment for the polypeptide backbone of interleukin 1β using three dimensional heteronuclear NMR spectroscopy. *Biochemistry 29*:3542–3556.

Eck MJ, Shoelson SE, Harrison SC. 1993. Recognition of a high-affinity phosphotyrosyl peptide by the src homology-2 domain of p56^{lck}. *Nature 362*:87–91.

Escobedo JA, Kaplan DR, Kavanaugh WM, Turck CW, Williams LT. 1991. A phosphatidylinositol-3 kinase binds to platelet-derived growth factor receptors through a specific receptor sequence containing phosphotyrosine. *Mol Cell Biol 11*:1125–1132.

Fantl WJ, Escobedo JA, Martin GA, Turck CW, del Rosario M, McCormick F, Williams LT. 1992. Distinct phosphotyrosines on a growth factor receptor bind to specific molecules that mediate different signaling pathways. *Cell 69*:413–423.

Felder S, Zhou M, Hu P, Urena A, Ullrich A, Chauduri M, White M, Shoelson SE, Schlessinger J. 1993. SH2 domains exhibit high-affinity binding to tyrosine-phosphorylated peptides yet also exhibit rapid dissociation and exchange. *Mol Cell Biol 13*:1449–1455.

Kashishian A, Kazlauskas K, Cooper JA. 1992. Phosphorylation sites in the PDGF receptor with different specificities for binding GAP and PI3 kinase in vivo. *EMBO J 11*:1373–1382.

Kay LE, Torchia DA, Bax A. 1989. Backbone dynamics of proteins as studied by ^{15}N inverse detected heteronuclear NMR spectroscopy: Application to staphylococcal nuclease. *Biochemistry 28*:8972–8979.

Koch CA, Anderson D, Moran MF, Ellis C, Pawson T. 1991. SH2 and SH3 domains: Elements that control interactions of cytoplasmic signaling proteins. *Science 252*:668–674.

Kraulis PJ. 1991. MOLSCRIPT: A program to produce both detailed and schematic plots of proteins. *J Appl Crystallogr 24*:946–950.

Main AL, Harvey TS, Baron M, Boyd J, Campbell ID. 1992. The three-dimensional structure of the tenth type III module of fibronectin: An insight into RGD-mediated interactions. *Cell 71*:671–678.

Maniatis T, Fritsch EF, Sambrook J. 1982. *Molecular cloning: A laboratory manual*. Cold Spring Harbor, New York: Cold Spring Harbor Laboratory Press.

Marion D, Ikura M, Tschudin R, Bax A. 1989. Rapid recording of 2D NMR spectra without phase-cycling. Application to the study of hydrogen exchange in proteins. *J Magn Reson 85*:393–399.

Messerle BA, Wider G, Otting G, Weber C, Wüthrich K. 1989. Solvent suppression using a spin lock in 2D and 3D NMR spectroscopy with H_2O solutions. *J Magn Reson 85*:608–613.

Norwood TJ, Boyd J, Heritage JE, Soffe N, Campbell ID. 1990. Comparison of techniques for ^{1}H-detected heteronuclear ^{1}H-^{15}N spectroscopy. *J Magn Reson 87*:488–501.

Otting G. 1993. Experimental NMR techniques for studies of protein–ligand interactions. *Curr Opin Struct Biol 3*:760–768.

Panayotou G, Bax B, Gout I, Federwisch M, Wroblowski B, Dhand R, Fry MJ, Blundell TL, Wollmer A, Waterfield MD. 1992. Interaction of the p85 subunit of PI 3-kinase and its N-terminal SH2 domain with a PDGF receptor phosphorylation site: Structural features and analysis of conformational changes. *EMBO J 11*:4261–4272.

Panayotou G, Gish G, End P, Truong O, Gout I, Dhand R, Fry MJ, Hile I, Pawson T, Waterfield MD. 1993. Interaction between SH2 domains and tyrosine phosphorylated PDGFb receptor sequences: Analysis of kinetic parameters by a novel biosensor based approach. *Mol Cell Biol 13*:3567–3576.

Pawson T, Schlessinger J. 1993. SH2 and SH3 domains. *Curr Biol 3*:434–442.

Sack RA. 1958. A contribution to the theory of the exchange narrowing of spectral lines. *Mol Phys 1*:163–170.

Schlessinger J, Ullrich A. 1992. Growth factor signaling by receptor tyrosine kinases. *Neuron 9*:383–391.

Shaka AJ, Barker PB, Freeman R. 1985. Computer-optimized decoupling scheme for wideband applications and low-level operation. *J Magn Reson 64*:547–552.

Shoelson SE, Sivaraja M, Williams KP, Hu P, Schlessinger J, Weiss MA. 1993. Specific phosphopeptide binding regulates a conformational change in the PI 3-kinase SH2 domain associated with enzyme activation. *EMBO J 12*:795–802.

Songyang Z, Shoelson SE, Chaudhuri M, Gish G, Pawson T, Haser WG, King F, Roberts T, Ratnofsky S, Lechleider RJ, Neel BG, Birge RB, Fujardo JE, Chou MM, Hanafusa H, Schaffhausen B, Cantley LC. 1993. SH2 domains recognize specific phosphopeptide sequences. *Cell 72*:767–778.

Waksman G, Shoelson SE, Pant N, Cowburn D, Kuriyan J. 1993. Binding of a high affinity phosphotyrosyl peptide to the src SH2 domain: Crystal structures of the complexed and peptide-free forms. *Cell 72*:779–790.